Dovepress

Open Access Full Text Article

ORIGINAL RESEARCH

Multifarious Biological Applications and Toxic Hg^{2+} Sensing Potentiality of Biogenic Silver Nanoparticles Based on *Securidaca inappendiculata* Hassk Stem Extract

Titilope John Jayeoye, [ID][1] Fredrick Nwude Eze,[2,3] Oladipupo Odunayo Olatunde,[4,5] Sudarshan Singh,[6] Jian Zuo,[7–9] Opeyemi Joshua Olatunji [ID][10]

[1]Department of Chemistry, Faculty of Physical Science, Alex-Ekwueme Federal University Ndufu-Alike, Abakalilki, Ebonyi State, Nigeria; [2]Faculty of Pharmaceutical Science, Prince of Songkla University, Hat Yai, Songkhla, 90112, Thailand; [3]Drug Delivery System Excellence of Center, Prince of Songkla University, Hat Yai, Songkhla, 90112, Thailand; [4]Department of Food and Human Nutritional Sciences, Faculty of Agricultural and Food Sciences, University of Manitoba, Winnipeg, MB, R3T 2N2, Canada; [5]Richardson Centre for Functional Foods and Nutraceuticals, University of Manitoba, Winnipeg, MB, R3T 6C5, Canada; [6]Food Technology and Innovation Research Center of Excellence, Institute of Research and Innovation, Walailak University, Nakhon Si Thammarat, 80160, Thailand; [7]Department of Traditional Chinese Medicine, The First Affiliated Hospital of Wannan Medical College (Yijishan Hospital), Wuhu, 241001, People's Republic of China; [8]Key Laboratory of Non-Coding RNA Transformation Research of Anhui Higher Education Institution, Wannan Medical College, Wuhu, 241001, People's Republic of China; [9]Research Center of Integration of Traditional Chinese and Western Medicine, Wannan Medical College, Wuhu, 241001, People's Republic of China; [10]Faculty of Thai Traditional Medicine, Prince of Songkla University, Hat Yai, 90110, Thailand

Correspondence: Opeyemi Joshua Olatunji
Faculty of Thai Traditional Medicine, Prince of Songkla University, Hat Yai, 90110, Thailand
Email opeyemi.j@psu.ac.th

Titilope John Jayeoye
Department of Chemistry, Faculty of Physical Science, Alex-Ekwueme Federal University, Ndufu-Alike (AE-FUNAI), P.M.B. 1010, Abakaliki, Ebonyi State, Nigeria
Email titilope12@gmail.com

Introduction: The use of environmentally benign resources for nanoparticles synthesis is consistently pushed to the front burner in a bid to ensure and enhance environmental protection and beneficiation. In this light, application of different plant parts for the reduction and stabilization of nanoparticles is gaining popularity.

Materials and Methods: In this contribution, we have exploited *Securidaca inappendiculata* stem extract (SISE), as the reducing and stabilizing agent for room temperature synthesis of highly stable and dispersed AgNPs. The major bioactive compounds in SISE were profiled using an ultra-high-performance liquid chromatography-quadrupole-time-of-flight mass spectrometry (UHPLC-MS-QTOF-MS).

Results and Discussion: SISE could reduce silver salts to its nanoparticles almost instantaneously with a maximum absorption spectrum at 423 nm, under the optimal conditions. The fabricated SISE AgNPs was extensively characterized using FTIR, TEM, SEM, XRD, EDS, Zeta analysis/DLS and TGA/DTG analysis. SISE AgNPs with average particles size between 10–15 nm and a zeta potential value of −19.5 ± 1.8 mV was obtained. It was investigated for in-vitro biological applications by carrying out, antimicrobial, antioxidant, hemolytic, cytotoxicity and antidiabetic assays. It was found that SISE AgNPs exhibited potent antimicrobial capacity against some food borne microbes, good antioxidant property, while also demonstrating high biocompatibility. Moreover, with a view to extending further the applications SISE AgNPs, it was tested as a colorimetric nanoprobe for Hg^{2+} detection in aqueous environment, where good linearity between 0.10 and 10.0 μM, with a detection limit of 26.5 nM, were obtained. The practicality of the probe was investigated by carrying out Hg^{2+} detection in water sample, with good accuracy and precision.
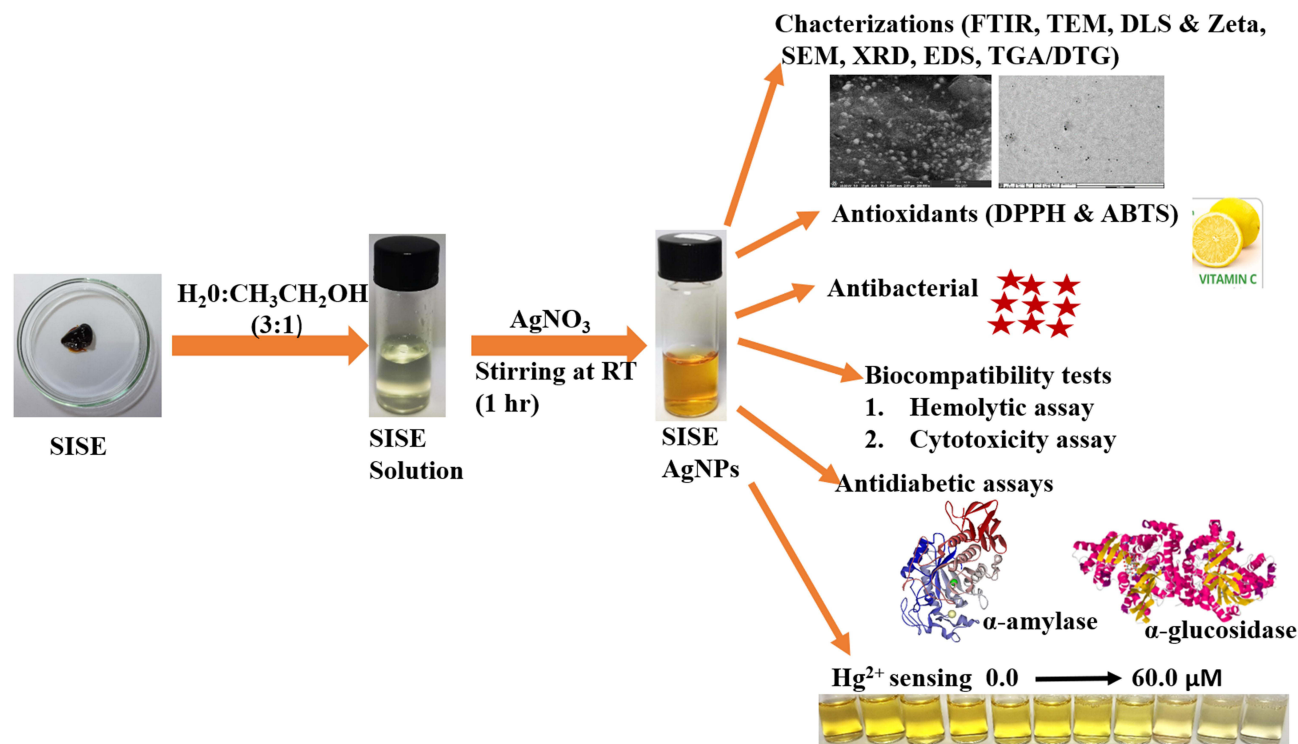
Discussion: Overall, this work introduced a new stabilizer for biocompatible AgNPs with far-reaching applications.

Keywords: silver nanoparticles, *Securidaca inappendiculata*, biological applications, mercury (II) ion, colorimetric probe

Introduction

Nano fabrication which deals with the ingenious synthesis of nanomaterials for wide ranging applications has gained much traction in the past few decades around the scientific community. This results from the limitless numbers of nanomaterials that can be produced from careful tuning of different synthesis conditions. In fact, according to the International Organization for Standardization (ISO), nanomaterial

Graphical Abstract

is defined as material with any external dimension in the nanoscale or materials with sizes in the range of 1–100 nm.[1] Amongst different kinds of nanomaterials available, silver nanoparticles (AgNPs) has received about the keenest interest, owing to its unique physico-chemical properties.[2] As a matter of fact, the use of silver as an antimicrobial agent dated back to antiquity, as silver skyphos (drinking cup) are common features in the Roman empire.[3]

The synthesis approach adopted in the fabrication of nanomaterials do have a direct effect in determining some physico-chemical property of the final product. Thus, chemical and biological synthesis are very popular. In chemical synthesis, the use of strong reductants such as: sodium borohydride, hydrazine, N, N dimethyl formamide etc,[4–6] have been well reported. Regrettably, the toxicity of some of the chemicals used for chemical-mediated nanoparticles synthesis has given rise to the call for more environmentally friendly methods. Biological synthesis of nanoparticles, where nature-friendly materials are sourced and used for nanofabrication has attracted a great deal of attention among scientists. Plant parts are a repository of bioactive metabolites and are thus keenly exploited for

nanomaterials fabrication. Some plants already used for AgNPs synthesis include: medicinal fern *Equisetum arvense*,[7] *Viburnum opulus* L. fruits extract,[8] *Centella asiatica* phenolic extract,[9] *Moringa citrifolia* L. (noni) different parts,[10] aqueous leaf extracts of *Lippia citriodora*,[11] etc. The use of other bio-based materials such as amino acids, bacterial isolates, fungus isolates and natural biopolymers, for other metal nanoparticles synthesis, all fall within the ambit of the "green synthesis."[12–18] The exceptional properties of AgNPs made it an efficient resource with applications already extended into diverse human fields of endeavors, ranging from; potent antimicrobial agents,[19] constituents of food packaging materials,[20] as components of medical sutures coatings,[21] in analytical detection of diverse analytes[22,23] and as a delivery agent of some drugs, in conjunction with its role in cancer therapeutics.[24]

As it is generally believed in the scientific community, the inherent metal toxicity of metal nanoparticles (MNPs), is an issue of great concern.[25] As a result, the use of biocompatible materials for MNPs synthesis is believed to be a practical mean of reducing the toxicity index of the final products.[26] In the same light, having found out from

literature, that *Securicaca inappendiculata* has not been reported for nano-fabrications, thus, we were motivated to fill this research gap by reporting the very first AgNPs from this highly important plant material.

Securicaca inappendiculata (Chan Yi Teng) is a Chinese medicinal plant native to southern Chinese provinces of Yunnan, Guangxi, Guangdong, and Hainan.[27] *S. inappendiculata* has been documented in ethno-medicine use for the treatment of fractures and rheumatoid arthritis.[28] Aside its use in traditional medicine, several pharmacological activities have been reportedly associated with the plant including antioxidant, antidiabetic, anti-inflammatory and antibacterial effects.[29,30] Numerous bioactive compounds particularly xanthones, triterpene saponins, benzophenones, xanthone glycosides, organic acids, neolignan glycosides, terpenoid glycosides, and phenolic compounds have been reported from the plant.[27,29,31] As a result, *S. inappendiculata* is highly rich in bioactive materials and as such should be effective for the reduction of metal salt for nano-synthesis.

Mercury (Hg) contamination of major environmental matrices is quite prevalent nowadays owing to diverse human activities with potentials for Hg emission. Mining and fossil fuel combustion account for a large percentage (60%) of the global Hg emission.[32] Artisanal small-scale gold mining account for another significant percentage, contributing to 20–30% of Hg pollution on earth.[33] Other major sources such as cement production, iron and steel production, mercury production and wastes disposal have been well documented.[34] The major forms of Hg include: elemental mercury (Hg^0), inorganic mercury (Hg^+ and Hg^{2+}), and organic mercury (CH_3Hg^+ and $C_2H_5Hg^+$). Amongst them Hg^{2+} has received huge interest in terms of method development, particularly based on the use of metal nanoparticles as optical probes. This is so, in view of the associated deleterious health impacts of Hg^{2+} consumption, which necessitated regular profiling in aqueous environment. Hg^{2+} can impart significant damages on the CNS, brain and kidney.[35] Methylation of Hg in aqueous environment to methylmercury (CH_3Hg^+) can bioaccumulate and bio-magnify across the trophic level, with possible high concentrations in animals like fish.[36] In view of the foregoing, the World Health Organization (WHO) maximum permissible limit of Hg^{2+} in drinking is fixed at 30 nM, while 10 nM, is the acceptable level by the United State Environmental Protection Agency (USEPA). Since the human tissues may be a final sink, for Hg^{2+} ingestion from water bodies, thus the detection of Hg^{2+} in aqueous

environment has received huge interest from researchers and thus our group is investigating this using an environmentally-friendly realized AgNPs as part of our objective for the current work. With considerable attention being devoted into environmentally benign nanofabrication, we therefore aimed at a SISE mediated synthesis of biocompatible AgNPs, which can be deployed for multifaceted human applications covering biomedical field, pharmaceutics and environmental science. The use of green synthesized nanoparticles for this wide spectrum applicability are not common, hence we hope this work will perfectly cover such research lacuna.

Herein, we have investigated the use of *Securicada inappendiculata* as a reductant of silver salt towards environmentally benign and sustainable synthesis of highly stable and dispersed AgNPs. *S. inappendiculata* is rich in bioactive compounds, which can effect almost instantaneous reduction of silver salt to AgNPs. We further investigated the biological properties of the fabricated SISE AgNPs by carrying out antibacterial, antioxidant, RBC hemolytic assay, cytocompatibility assay using normal human embryonic colon cells (Caco-2) and mouse fibroblast (L-929) cells. The inhibition of SISE AgNPs on common enzyme, implicated in the management of diabetes (α-amylase and α-glucosidase), were equally investigated. Finally, SISE AgNPs was tested as a colorimetric nanoprobe for the detection of toxic Hg^{2+} in aqueous environment, with reliable analytical performance indices. In all, SISE AgNPs was found to show great promise as a potential biomedical resource, while also exhibiting satisfactory performance as a probe in environmental management of heavy metal contamination profiling in environmental sample.

Materials and Methods
Materials

Potassium persulfate were purchased from Sigma-Aldrich, Inc. (St. Louis, MO, USA). Also, 2,2-azino-bis-(3-ethylbenzothiazoline-6-sulfonic acid) diammonium salt (ABTS) and 2,2diphenyl-1-picrylhydrazyl (DPPH) were obtained from Fluka Chemicals (Buchs, Switzerland) and Aldrich Chemical Company (Steinheim, Germany) respectively. Tryptic soy agar (TSA), phosphate-buffered saline (PBS), and TSB (tryptic soy broth) were procured from Oxoid (Hampshire, England). Metal salts for sensing and selectivity tests include: $HgCl_2$ from VWR chemicals BDH, $FeSO_4.7H_2O$ from Merck, $FeCl_3.6H_2O$, $MgCl_2.6H_2O$ and

$NiCl_2.6H_2O$ were procured from Loba Chemie, $ZnSO4.7H_2O$, $Al(NO_3)_3.9H_2O$, $CdCl_2.2.5H_2O$, $Ca(NO_3)_2.4H_2O$, $CuSO_4.5H_2O$, $CoCl_2.6H_2O$, were all from UNIVAR APS FineChem, while KNO_3 and $Pb(NO_3)_2$ were procured from ANAPURE.

Plant Material and Extract Preparation

The stems of *S. inappendiculate*, were purchased from Bozhou Medicinal Herbs Market, Anhui Province, PR China. The authentication of the plant was done by Dr Jian Zuo (Department of Traditional Chinese Medicine, The first Affiliated Hospital of Wannan Medical College, China). A voucher specimen with the reference number ID: 2017-11-034 was deposited at the herbarium of the Department of Traditional Chinese Medicine, Wannan Medical College. Further study approval on the use of the plant were not required, according to regional and institutional guidelines. The dried stems of *S. inappendiculata* (2 Kg) was subjected to extraction using 95% ethanol. The extracts were filtered and dried. The dried extract was further subjected to one round of re-extraction using 50% ethanol. The extract was dried using a rotary evaporator and the crude ethanol extract, coded (SISE) was stored at 4°C until further use.

UHPLC-ESI-QTOF MS Characterization of *S. inappendiculata* Stem Bark Extract (SISE)

Qualitative UHPLC-DAD-ESI-QTOF-MS/MS an anlysis of *S. inappendiculata* stem bark extract was performed to determine the tentative identities of the secondary metabolites present. Briefly, 50 mg of the sample was dissolved in 1 mL of 70% methanol. The mixture was vortexed and then centrifuged for 5 min at 7168 xg. The supernatant was subsequently filtered through a 0.2 µm nylon membrane syringe filter. The filtrate was then used for LC-MS analysis as described in our previous report.[9]

Synthesis of SISE AgNPs

Synthesis of SISE AgNPs was carried out based on our previous report,[9] with modifications. 5.0 mg/mL of SISE was prepared in a mixture of water:ethanol (3:1). Into a 100 mL beaker, which was wrapped round with aluminum foil to avoid light induced oxidation of the reaction mixture, 95 mL of different concentrations of $AgNO_3$ solution was added under stirring at room temperature (RT). Then 5.0 mL of SISE aqueous solution, whose pH

has been adjusted to 10.0, using few drops of 0.5M NaOH solution was added. The mixture was continuously stirred for 1 hr and was stored at 4 °C before clean-up. The synthesized SISE AgNPs was centrifuged at 25,200 xg on a temperature-controlled centrifuge for 30 min in order to obtain the particles pellets. The pellets were washed by subjecting to two more rounds of centrifuging and re-suspension in ultra-pure water. Finally, the pellets were freeze-dried and subjected to instrumental characterizations. The synthesis protocol was optimized by changing the concentrations of $AgNO_3$ solutions used. The photo images and absorption spectra were collected using a spectrophotometer and Samsung Galaxy phone A50s.

Characterizations of SISE AgNPs

The absorption spectra of SISE AgNPs was acquired on a JASCO V-730 Spectrophotometer (Germany), functional groups interaction between SISE and SISE AgNPs were elucidated using a Fourier-transformed infrared spectroscopy (FT-IR), with wavelength covered between the region of 4000 to 500 cm^{-1} on a Spectrum BX PerkinElmer FTIR spectrometer, particles images were observed using a Transmission electron microscope (TEM), JEM 2010 (JOEL, Japan) and a field emission scanning electron microscopy (FESEM), linked to an energy dispersive X-ray spectroscopy (EDX), on a SEM microscope, Apreo, FEI (Czech Republic), with a EDX machine (X Max 80, Oxford Instrument, United Kingdom). Particle crystallinity was investigated using an Empyrean XRD diffractometer (Empyrean, Netherland), acquiring the $2(\theta)$ from 10 to 80° using Cu Kα, using a radiation wavelength of 0.154 nm and a scan speed of 70.2 s. Particles' hydrodynamic diameters and zeta potential were obtained using Brookhaven NanoBrooks zetaPALS (Brookhaven, instrument, USA). Thermal gravimetric analysis (TGA) and derivative thermal gravimetric analysis (DTG), of SISE AgNPs were obtained on a TGA7 (Perkin Elmer, USA), by heating a small fraction of SISE AgNPs pellets from 50 to 1000 °C at 10.0 °C/min under nitrogen atmosphere.

Antioxidant Capacity of SISE AgNPs
DPPH Radical Scavenging Activity of (DPPH-RSA)

Radical scavenging activity of SISE AgNPs was carried out following our previous work with slight modifications.[37] Briefly, 150 µL of SISE AgNPs or standard ascorbic acid aqueous solution (10 to 40 µg/mL) was pipetted into 96-well microplate. DPPH already prepared

in methanol (150 µL, 0.1 mM) was added into the sample solutions with thorough mixing. The absorbance was acquired at 517 nm after allowing the reaction to incubate for 30 min at room temperature. The DPPH radical scavenging activities was expressed as percentage inhibition.

DPPH radical scavenging effect (%) = [(Ac − As)/Ac] × 100 where, Ac is the absorbance of the control, and As is the absorbance of the sample or standard.

ABTS Radical Scavenging Activity

The ABTS radical scavenging activity of SISE AgNPs was carried out following our previous report,[13] where the details of the experimental steps are reported.

Antibacterial Capacity of SISE AgNPs
Bacterial Cultures and Cell Suspensions

Staphylococcus aureus, DMST 4745, *Escherichia coli* DMST 4212, *Vibrio parahaemolyticus* PSU.SCB.16S.14, *Listeria monocytogenes* F2365, and *Pseudomonas aeruginosa* PSU.SCB.16S.11 were collected from the Food Microbiology Laboratory. All bacteria strains were gifted by the Food Safety Laboratory, department of Food Technology, Prince of Songkla University, Hat Yai, Thailand. Bacterial suspensions were prepared following the method reported by Olatunde et al.[38] Bacterial load in sterile PBS was diluted to 6 log CFU/mL.

Minimum Inhibitory Concentration (MIC) and Minimum Bactericidal Concentration (MBC)

The MIC and MBC of SISE AgNPs against selected bacteria were determined following the procedure outlined in previous work with minor modification.[38]

Biocompatibility Studies
Hemolytic Effect of SISE AgNPs on Human Red Blood Cells

Hemolytic effect of SISE AgNPs was determined on viable human erythrocytes as described in previous publications.[13,39,40] After written Informed Consent was provided by the individual, blood sample was collected from one of the authors (Dr. Titilope J. Jayeoye), as donor by venipuncture. The freshly collected sample was washed by suspending in phosphate buffered saline (PBS), pH 7.4 followed by centrifuging at 112 xg for 5 min. The supernatant and buffy coats were discarded. After three rounds

of washing, the erythrocyte pellet was resuspended in PBS to a final concentration of 5% (v/v). Different concentration SISE Ag NPs (100 µL) were added to 400 µL of erythrocyte solution. Samples containing Triton X-100 (1% in PBS) were used as positive control while those with only PBS served as negative control. After 1 h of incubation at 37 °C, the samples were centrifuged at 112 xg at room temperature. Supernatants were collected and the absorbance read at 540 nm. The results obtained were presented as % hemolysis. The Ethics Committee of the Alex Ekwueme Federal University (AE-FUNAI), with approval detail (EC-AFUNAI-141/2020), granted permission for the use of human serum.

Effect of SISE AgNPs on Human Embryonic Colon Cell and Fibroblast Cell

The cyto-compatibility of SISE AgNPs was assessed on human embryonic colon cells (Caco-2) and mouse fibroblast cells (L-929) independently three times. Caco-2 and L-929 cells were cultured in high glucose Dulbecco's Modified Eagle Medium (DMEM) containing 10% fetal bovine serum and 1% penicillin-streptomycin solution (Gibco). Briefly, 4×10^4 cells/mL of CaCo-2 and L-929 were seeded into a 96-well plate and incubated at 37 °C with 5% CO_2 atmosphere for 24 h. Cells were treated with 100 µL of varying concentrations of SISE AgNPs (-26.875–0.209 µg/mL) and incubated for 24 h. The concentration of SISE AgNPs was adopted for cytocompatibility test was based on the results of the antibacterial assay, with the maximum concentration being more than three times the MIC value. The viability of cells after treatment was analyzed using MTT assay and the optical density measured (OD) at 570 nm.

$$\text{Percentage cell viability} = \frac{\text{OD Treatment}}{\text{OD Control}} \times 100$$

Antidiabetic Property of SISE AgNPs
Determination of α-Amylase Inhibitory Activity

The porcine pancreatic α-amylase inhibitory activity determination procedure was done by using slightly modified method from Chakrabarti et al[41] and Sudha et al.[42]

Determination of α-Glucosidase Inhibitory Activity

The α-glucosidase inhibitory activity determination process was performed using slightly modified procedure from Kumar et al.[43]

SISE AgNPs as Colorimetric Probe for Hg^{2+} Detection in Aqueous Solution

For Hg^{2+} detection using SISE AgNPs, briefly, into a 5 mL tube, 200 μL of SISE AgNPs was added, followed by the addition of 1600 μL ultra-pure water. Then 200 μL of different concentrations of Hg^{2+} ion solution was injected. The mixture was vortex mixed and allowed to incubate for 5 min after which the absorption spectra and photo images were collected using a spectrophotometer and Samsung phone A50s respectively. The final concentrations of Hg^{2+} in the 2.0 mL reaction mixture ranged within 0.10–60.0 μM.

Results and Discussion
UHPLC-ESI-QTOF MS Profiling of *S. inappendiculata* Stem Bark Extract (SISE)

The biosynthetic capacity of plant extracts depends on the content and type of secondary metabolites present. Some class of plant bio-actives have shown to be highly efficacious as reducing and/or stabilizing agents compared to others.[44] Thus, it is pertinent to the know the type of metabolites present in plant extract intended for biogenic synthesis of metal nanoparticles. The putative identities of the individual compounds found in the extract of *S. inappendiculata* stem bark was determined using UHPLC-ESI-QTOF-MS analysis in the negative ionization mode, as previously reported in our earlier investigation.[45] Moreover, previously documented reports had alluded to the presence of xanthones and phenolics in *S. inappendiculata*. The negative ion mode was adopted considering its good sensitivity towards xanthones and even better sensitivity towards phenolics vis-à-vis the positive mode. Considering the good sensitivity of xanthones, and even better sensitivity of phenolics in the negative ionization mode. The base peak chromatogram of the extract revealed majority of the compounds were eluted within 21 min and the different peaks suggest the presence of different compounds (Figure S1). The putative identities of these compounds, retention time, exact mass, chemical formula, score, mass error (within ± 5 ppm) are presented in Table S1. It is apparent that most of the compounds obtained were present as glycosides. Phenolics constitute the majority of the compounds and these included flavonoids, phenolic glycosides, phenolic lipids and xanthone glycosides. Some of these compounds
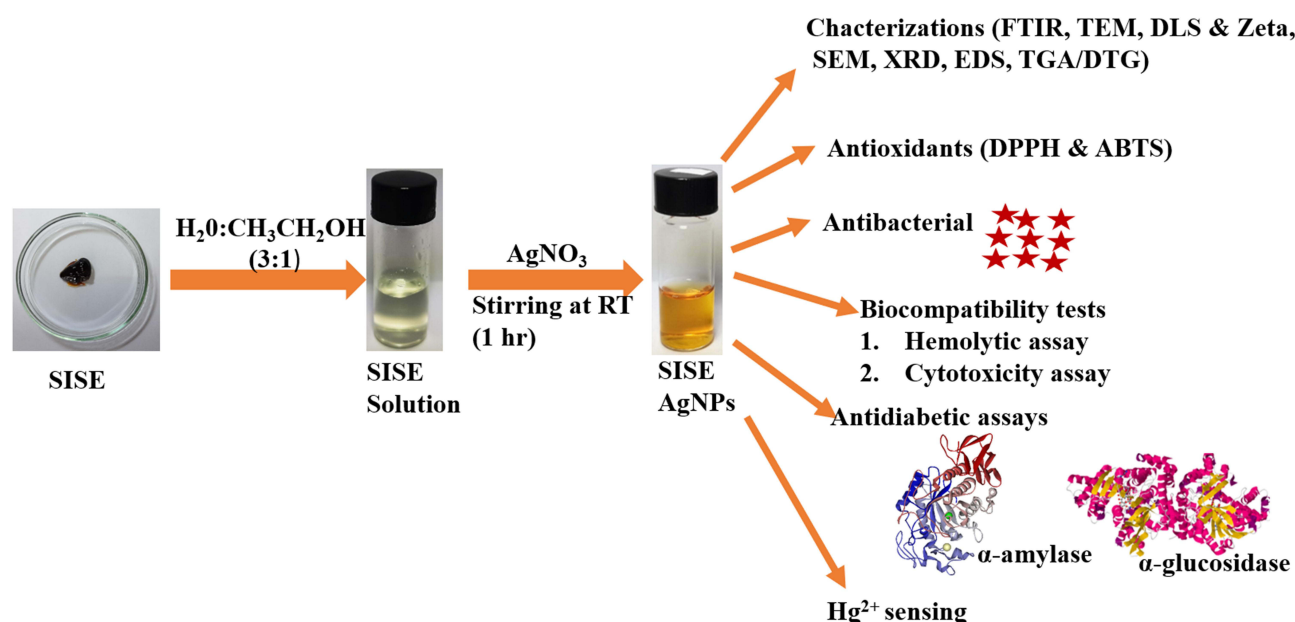
have previously been reported to possess strong antioxidant activities.[46,47] Given the strong positive correlation that exist between antioxidant ability of bioactive compounds and their capacity for reductive biosynthesis of metallic nanoparticles, the presence of these compounds in *S. inappendiculata* stem bark extract is a good indication of its potential viability for green synthesis.

Synthesis of SISE AgNPs

Room temperature synthesis of SISE AgNPs was conducted by mixing pH adjusted SISE solution to pH 10.0 (using NaOH solution) and AgNO$_3$ under stirring. The synthesis protocol and the applications of the fabricated SISE AgNPs in this work, is shown in Scheme 1. Our objective was to realize a nanomaterial with potential applications especially in biomedical and environmental fields.

Since the synthesis process is dependent on the concentrations of AgNO$_3$ used, the concentration of AgNO$_3$ was optimized from the outset. As shown in Figure 1, the absorbance maximum of the nanoparticles realized, under different concentrations of AgNO$_3$ are as follows. 1.0 mM (425 nm), 2.0 mM (427 nm), 3.0 mM (423 nm), 4.0 mM (425 nm) and 5.0 mM (426 nm). In all, sharp absorption spectra are obtained, while color transition of colorless AgNO$_3$ to sparkling yellow color, which is characteristic of small sized AgNPs are furnished (Figure 1 inset). Further, since the absorbance maximum can be used to predict the particle sizes of nanoparticles,[48] AgNO$_3$ concentration at 3.0 mM, furnished the shortest absorbance maximum and was selected at the optimized concentration for this work. The role of NaOH on the synthesis process was investigated and depicted in Figure S2. As shown, the photo images and the absorption spectra of AgNO$_3$ salt (Figure S2(A)), AgNO$_3$ salt and NaOH mixture (Figure S2 (B)) and the mixture of AgNO$_3$ salt, NaOH and SISE (Figure S2(C)), clearly shows that nanoparticles formation in the presence of NaOH alone is non-feasible. It was only the mixture of AgNO$_3$ salt, NaOH and SISE (Figure S2 (C)), that a sparkling yellow color of SISE AgNPs was obtained, which undoubtedly confirmed the role of SISE metabolites as the reductant and not NaOH.

The AgNPs synthesis success was profiled by monitoring the absorption spectra of the optimized concentration, under time frame of 75 min. As displayed in Figure S3, the absorption spectra remained unchanged after less than 15 min, while the synthesis kinetics obtained through a plot of A_{423} against Time (Figure S4), saturated quite fastly. This

Scheme 1 Schematics of SISE AgNPs synthesis, for diverse biological applications and Hg^{2+} sensing.
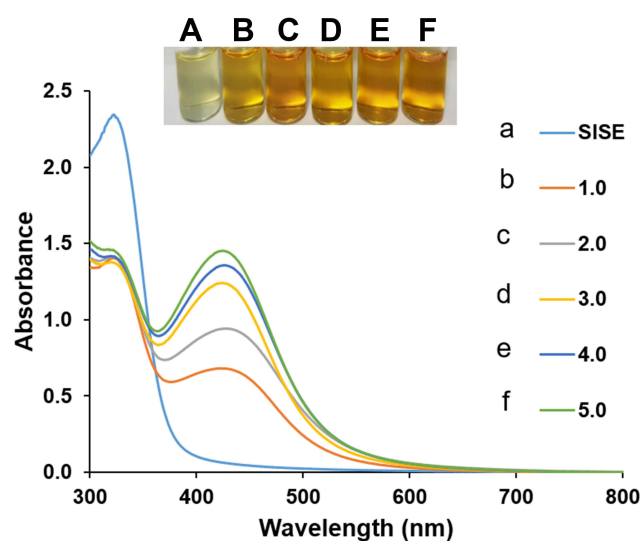

Figure 1 UV-V is absorption spectra of SISE AgNPs synthesis under different concentrations of AgNO$_3$, (a) SISE (b) 1.0 (c) 2.0 (d) 3.0 (e) 4.0 (f) 5.0 mM, inset shows the photo images.

is a proof of the reductive capacity of SISE, arising from the multitudinous bioactive metabolites present. For full completion of the nucleation and growth process of the nanoparticle's synthesis, we adopted synthesis time of 1 hr (60 mins), after which the synthesized nanoparticles were stored at 4 °C.

The mechanistic basis of SISE mediated synthesis is explained as follows. The addition of NaOH solution to SISE, will ensure that the bioactive constituents (xanthones and phenolics) are deprotonated, furnishing negative charges on their structures. The addition of AgNO$_3$ salt (Ag$^+$), will be firmly attracted to the bioactive materials. As a result, rapid redox reaction is subsequently set off, where electrons for the reduction of Ag$^+$ is provided by the bioactive materials. The synthesis of metal nanoparticles generally follows three notable stages viz: formation of seed, nucleation/growth stage and particles maturation stage through the Ostwald ripening process.[49,50] In the present SISE mediated synthesis of AgNPs, the seed formation stage is so rapid that observable color change of AgNO$_3$ solution was immediately noticed just after the addition of SISE solution, under stirring at room temperature (RT). At the nucleation/growth stage, the multitudinous Ag^0 served as catalyst for more reduction of Ag$^+$, as a result, more of AgNPs are formed, while further stirring ensured that the particles are grown into maturation and subsequently stabilized by plethora of the identified bioactive constituents in Table S1. Taking Eriodyctiol as a putative bioactive constituent of SISE, the mechanistic reduction of AgNO$_3$ is depicted in Figure 2. Accordingly, Ag$^+$ will bind to the free OH groups, after which it is reduced to Ag^0, while Eriodyctiol is oxidized to its ketonic equivalent. At the nucleation stage, Ag$^+$ are bound to the free OH groups of Eriodyctiol, after which the energy for the reduction of Ag$^+$ is supplied by the metabolite, very rapidly, AgNPs seeds are formed (Stage I). At stage II, the already formed
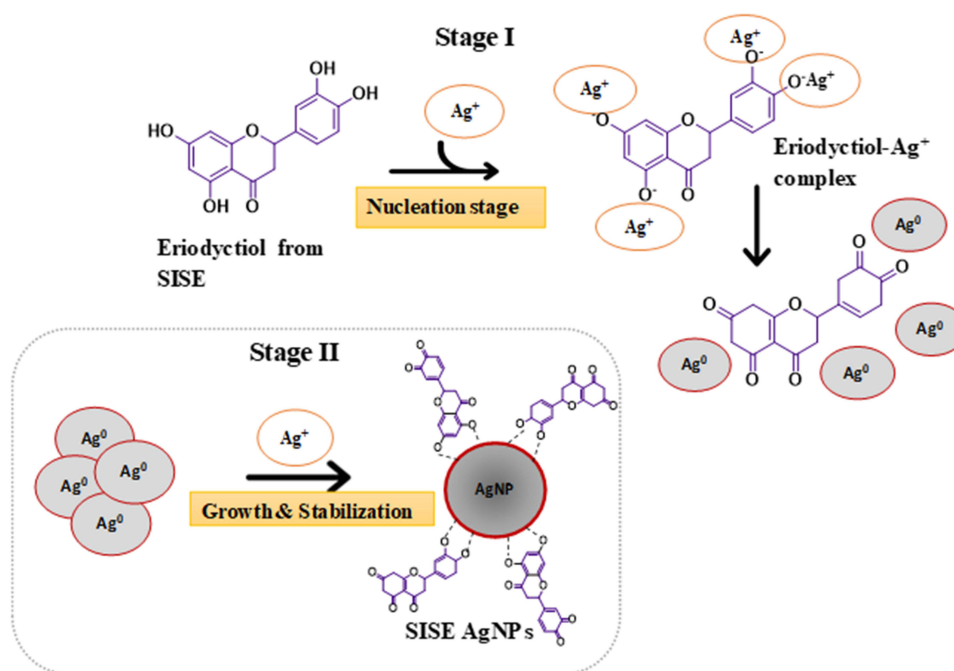
Figure 2 Mechanism of SISE AgNPs synthesis, using Eriodyctiol as a putative bioactive metabolite from SISE.

seeds are further attacked by more Ag^+ in solution, resulting in further reduction and formation of more nanoparticles. This circle continues until all the reductant are exhausted. The particles grow, mature and are finally stabilized by Eriodyctiol and other bioactive metabolites.

Characterization of SISE AgNPs

Detailed instrumental characterizations of SISE AgNPs were conducted in order to gain informed knowledge on the morphological properties of the synthesized nanoparticles. Figure 3A shows the FTIR spectrum of SISE (Figure 3A(a)), with notable peaks at 3320, 2900, 1620, 1410, 1162 and 932 cm^{-1}. These peaks can be ascribed to the C-H stretching vibration of OH groups, which is characteristic of flavonoids and phenolics, C-H stretching of aliphatic compounds (2900 cm^{-1}), C=O stretching of amides and C=C from active phyto-constituents in SISE (1620 cm^{-1}).[51] The peak at 1410 cm^{-1} is assigned to the C-C stretching of ringed form aromatic compounds, while the peaks at 1162 and 932 cm^{-1} are attributed to the C-O-C and C-OH stretching vibrations of some notable secondary alcohols. The identified peaks in SISE AgNPs (Figure 3A(b)), are located at the wavelengths, 3420, 2910, 1590, 1390 and 1060 cm^{-1}. As observed, they are all shifted in comparison with those profiled in SISE, which indicated the interaction between SISE and the

synthesized AgNPs. These similar peaks have been identified in our previous works.[9,52]

The TEM images of SISE AgNPs are displayed in Figure 3B. As can be clearly seen, the images are spherical and highly dispersed, attesting to the stability of colloidal solution. The TEM images at higher magnification (50 nm) is shown in Figure 3C. The particles are monodispersed with similar sizes. This shows that the seed formation stage and the particles maturation stage during the nanoparticle's synthesis occurred almost spontaneously, arising from the high reductive capacity of SISE in reducing silver salt to its nanoparticles. The histogram of the particles' sizes is shown in Figure S5. It revealed that the particles are well distributed between 10–15 nm, which falls within the range of size distribution particularly of interest in biological assays. The particle size was further investigated using the dynamic light scattering (DLS) machine, which measures the sizes of nanomaterials in solution. As shown in Figure 3D, shows a DLS size of 37.5 ± 2.5 nm, with polydispersity index (PDI) of 0.218. This size was much higher than the sizes from TEM, owing to the fact that DLS measurements are carried out in aqueous environment, as a result, there exist a tendency of measuring the hydration shell of water molecules surrounding the particles unlike TEM, where measurements are conducted on already dried surfaces. The PDI value obtained validated the images observed from TEM,
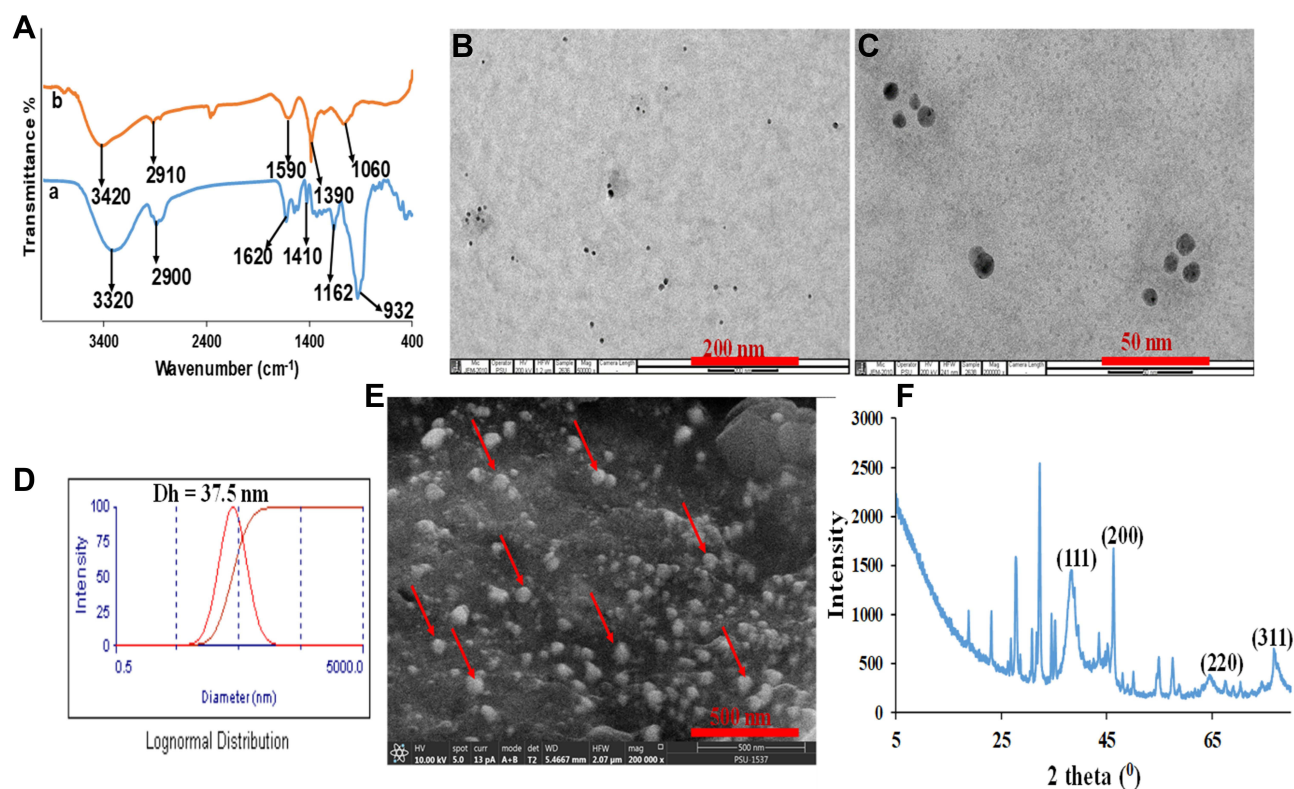
Figure 3 (**A**) FTIR of (a) SISE (b) SISE AgNPs (**B**) TEM (200 nm) (**C**) TEM (50 nm) (**D**) Hydrodynamic diameter from DLS (**E**) FESEM (**F**) XRD of SISE AgNPs.

showing that the particles are of monodispersed morphology. The FESEM images of SISE AgNPs are revealed in Figure 3E. As can be seen, white specs of AgNPs are conspicuous on the surface, as marked by the red arrows. The particles are spherical and of similar shape, just similar to the images from TEM. The x-ray diffraction (XRD) of SISE AgNPs is shown in Figure 3F. The characteristic crystalline facets of Ag are displayed with 2 theta (^{0}), positions of 38.52, 46.35, 64.50 and 76.95°, which are assigned to the (111), (200), (220) and (311) of face centered cubic, *fcc* crystallographic structure of AgNPs, using 01-071-3762 reference code from library. The other conspicuous peaks not assigned may have resulted from the crystallization of SISE stabilizer on the fabricated AgNPs surfaces, which further validated the presence of bioactive compounds on the nanoparticles' surfaces. The Scherer equation was used to estimate the crystallite size of SISE AgNPs using the equation, $[L= \lambda/\beta cos\theta]$, where L represent the crystallite size, k is a constant 0.9, λ is the wavelength of the X-ray radiation source, while β is the angular full width at half maximum (FWHM) of the most prominent peak of the XRD spectrum of the nanoparticles, at diffraction angle θ. The estimated average crystalline size of SISE AgNPs was calculated to be about 17.3 nm, which is quite close to the size distribution of 10–15 nm estimated from TEM. The Energy Dispersive X-ray spectroscopy (EDS) analysis of SISE AgNPs, which can reveal the surface morphological features of the nanoparticles is displayed in Figure S6. Sharp and intense peak of Ag at 3.0 keV, with presence of carbon and oxygen peaks are clearly observed. The major identified elemental compositions of SISE AgNPs, revealed Ag (77.8%), C (13.6%) and O (8.6%). Which confirmed that the reductant effected good synthesis of a stable and dispersed nanoparticles. The elemental mapping from EDS is shown in Figure S7, which validated the presence of Ag, C and O. Further, the thermogravimetric analysis (TGA) and differential thermogravimetric analysis (DTG) plot of SISE AgNPs is shown in Figure S8. As can be seen, three major stages can be identified in the TGA plot (Figure S8 A). These stages are detailed in Table S2 as, stage I (41.75–169.81), with the onset at 41.75 °C, stage II (169.71–662.22), with the onset at 169.71 °C, and stage III (662.22–1010.00), with the onset at 662.22 °C. Stage I is attributed to the loss of moisture, stage II is a result of the degradation of carbonaceous materials, while stage III is the total

decomposition stage, equally tagged the ash stage. The percent ash of 59.5% of SISE AgNPs at 1010 °C, attest to the heat stability and robustness of the fabricated nanoparticles. This similar TGA profile has been reported by Okaiyeto et al.[51] The DTG profile of SISE AgNPs (Figure S8 B), is reflective of the various stages identified in the TGA profile.

In all, extensive characterizations of SISE AgNPs confirmed stable, monodispersed particles with particles' sizes suitable for multifarious applications in both biomedical and environmental field.

The Antioxidants Activity of SISE AgNPs

The antioxidant property of SISE AgNPs investigated using the DPPH-RSA and ABTS-RSA assays is shown in Figure 4A and B, respectively. As shown, SISE AgNPs exhibited comparable activity with ascorbic acid (AA) standard. The antioxidant activities of nanoparticles, particularly those synthesized by plant extract have been documented. AgNPs synthesized using the outer peel extract of *Ananas comosus* showed promising ABTS-RSA and DPPH-RSA in a dose dependent manner.[7] The antioxidant potentiality of SISE extract had been investigated and reported in our previous work,[45] and thus not repeated here. These antioxidant activities can be associated with the phenolic and other numerous bioactive compounds present in the plant extracts, which can donate hydrogen or protons to free radicals and thus terminating the chain reaction of oxidation.[53] Hydrogen or protons can be donated by the several hydroxyl groups in the benzene ring of the

different phenolics contained in the extract.[54] El Batal et al[55] attributed the antioxidant activities of zinc NPs to ZnNPs capped with biological contents, particularly phenolic compounds, which possess the free radical scavenging activity. Generally, the antioxidant properties of polyphenols are lower than polyphenols-capped metal nanoparticles, suggesting that the increase chemical properties of the nanoparticles may be due to synergistic effects from the encapsulating bioactives and the metal nanoparticles.[56] Previously, de Souza et al, observed a higher antioxidant activity of flavonoid-metal complexes relative to the individual components.[56] The authors attributed this observation to the acquisition of additional superoxide dismutating centers the complex. SISE is endowed with phenolics, but the "complex" in the present study is a small-sized metalNP (10–15 nm). Thus, it is more plausible that the observed higher antiradical activity of SISE AgNPs may be related to the increase in surface area-to-volume ratio which afforded the encapsulating bioactives with larger active surface for effective radical quenching underpinned by rapid electron transfers and valence transition. Similar synergistic antioxidant action by phyto-synthesized AgNPs was previously observed by Yousaf et al in the radial scavenging effect of Achillea millefolium L. extract synthesized silver nanoparticles.[19]

Thus, the antioxidant study revealed that SISE AgNPs could serve as an antioxidant agent, which might be helpful in combating some deleterious conditions associated with oxidative stress or reactive radicals' generation.
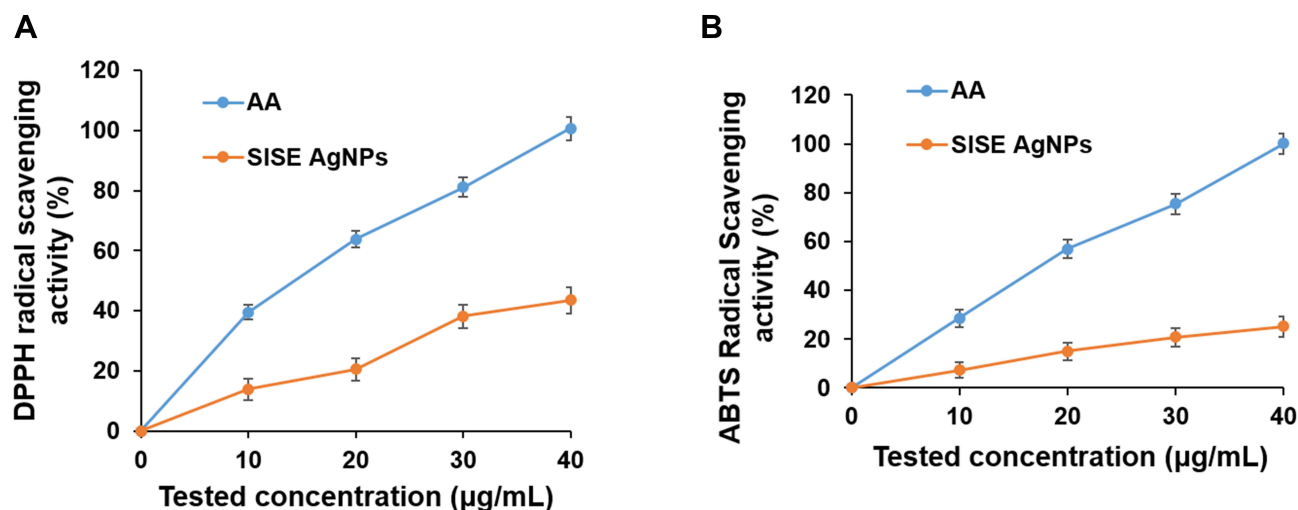

Figure 4 (**A**) DPPH radical scavenging and (**B**) ABTS activity of SISE AgNPs, in comparison with standard Ascorbic acid (AA).

Table 1 Antimicrobial Activity of SISE AgNPs

Bacterial Strains	Minimum Inhibitory Concentration (MIC) (µg/mL)	Minimum Bactericidal Concentration (MBC) (µg/mL)
P. aeruginosa	2	2
E. coli	2	4
V. parahaemolyticus	2	2
S. aureus	4	8
L. monocytogenes	2	8

Note: Values represent mean (n = 3).

Antimicrobial Activity of SISE AgNPs

SISE AgNPs showed great inhibition towards both Gram-negative bacteria (GNB) and Gram-positive bacteria (GPB), with MIC and MBC values ranging from 1 to 4 µg/mL and 2 to 8 µg/mL, respectively (Table 1). The electrostatic interaction between positively charged nanoparticle and the negatively charged bacterial surface, which can induce alteration in the outer membrane integrity of bacteria as well as leakage of cytoplasmic contents, is often adduced as the mechanistic basis of the antimicrobial properties of AgNPs.[57] Similarly, positive ions released by nanoparticle could interact with the negatively charged components (sulphur and phosphorus) of bacterial DNA, and binds with the double-stranded DNA, leading to the disordering of the helical structure by cross-linking within and between the nucleic acid strands. Thus, inducing stress and ultimately bacterial death.[58] However, the fabricated SISE AgNPs is negatively charged, hence electrostatic interaction may not hold as the basis of interaction with bacterial cells. It is safer to reason that the proximity of SISE AgNPs to the bacterial cells in aqueous solution may trigger the release of some secretions to the surrounding milieu, which will facilitate the leaching of Ag^+. Moreover, the high surface area to volume ratio of SISE AgNPs, can enhance the passage of SISE Stabilizers on the nanoparticles into the bacterial cells, providing synergistic combinations of SISE on one hand and deleterious Ag^+ on the other hand, which may be responsible for bacterial inactivation.[59] The inner and outer membrane of the bacterial cell can be partitioned by their interaction with phenolics, thus rendering them membrane permeable,[60] which may further facilitate the penetration of the released ions from nanoparticles. Qais et al[61] reported that antimicrobial properties of AgNPs synthesized using *Murraya koenigii* leaves against extended-

spectrum β-lactamase-producing enteric bacteria and methicillin-resistant *Staphylococcus aureus* was attributed to the attack of AgNPs on the bacterial cell's respiratory chain and cell division. From the result in Table 1, the MIC and MBC were higher for GPB as compared to GNB. These findings were in agreement with the report of Jayeoye et al[62] who documented a lower resistance for GNB against AgNPs synthesized using 3-aminophenyl boronic acid as compared to GPB. This could be associated with the differences in their varying membrane structure between GNB and GPB. Acharya et al[63] attributed differences in cell wall compositions as the basis of high resistivity of GPB to both spherical and rod-shaped AgNPs in comparison to GNB. The outer membrane of GPB is composed of several layers of peptidoglycan as compared to the single layer of peptidoglycan in GNB, which could justify the high resistivity of GPB towards AgNPs.[63]

Biocompatibility of SISE AgNPs
Hemolytic Assay

Cyto-compatibility of metal nanoparticles is always an important issue of consideration when evaluating their viability. This is more so given that metal nanoparticles have in the past demonstrated considerable toxicity and thus pose serious potential concerns over environmental and human health risk. Hemolysis of erythrocytes is a simple and reliable approach to quickly obtain basic insights about the biocompatibility of nanomaterials. The effects of SISE Ag NPs on human erythrocyte hemolysis are presented in Figure 5A. The erythrocytes sample incubated with Triton X-100 revealed massive hemolysis within 1 h adjudicated by the release of hemoglobin. RBC hemoglobin release by Triton-X 100 was due to membrane rupture as a result of increased permeability.[64] In contrast, the extent of erythrocyte hemolysis induced by both nanoparticles was far lower (less than 10%) as shown in Figure 5A. As previously outlined in the guideline for in vitro hemolysis proposed by Liu J et al,[36] that erythrocyte hemolysis of less than 10% should be considered non-hemolytic. Although the present data does not necessarily establish a complete absence of cytotoxicity by these nanoparticles,[65] it however indicates that they do not pose any risk of hemolysis and are likely cyto-compatible.

Cyto-Compatibility Assay on SISE AgNPs

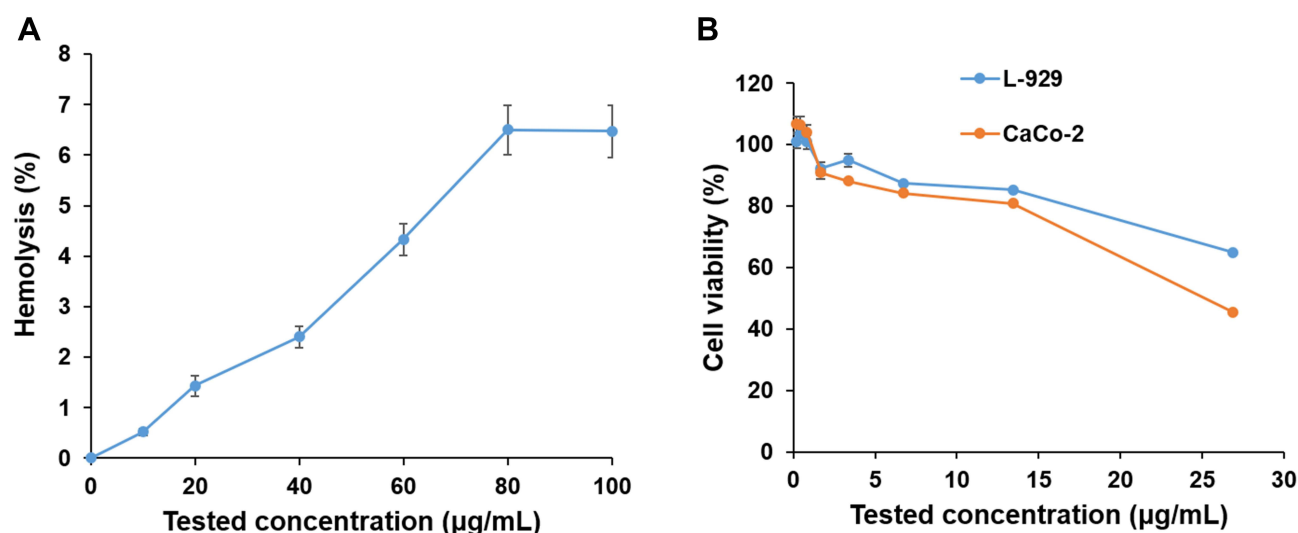Thousands of different nanoparticles are involved in our daily life with various origins from food, cosmetics,

Figure 5 (**A**) Effects of SISE AgNPs on erythrocyte hemolysis and (**B**) Cytotoxicity effects of SISE AgNPs on the viability of mouse fibroblast cells (L-929) and human embryonic colon cells (CaCo-2) at different concentration (0.209–26.875 μg/mL). Error bars represent the standard deviation of two measurements.

diagnosis, therapy, etc. It is believed that decreasing the size of materials up to nanometer can facilitate their unfavorable absorption since they can pass the biological barriers.[66] Hence, assessing the biocompatibility of synthesized SISE AgNPs targeted for biological usage was deemed necessary. The cyto-compatibility of metallic nanoparticles broadly depends on their shape, size, and aggregation behavior which is mostly affected by pH and electrolyte concentration. The synthesized SISE AgNPs were investigated for their cytotoxicity against Caco-2 and L-929 cells at a range of (0.209–26.875 μg/mL). The results of cytotoxicity (Figure 5B) demonstrated concentration dependent toxicity for synthesized SISE AgNPs. Moreover, the SISE AgNPs at tested concentration of 13.43 μg/mL showed > 80% of cell viability for Caco-2 and L-929 cells lines. Similar studies on AgNPs have been previously demonstrated biocompatible with Caco-2 and HEK293T cells.[67]

Antidiabetic Property of SISE AgNPs

Diabetes, a metabolic disease characterized by excessive hyperglycemia with devastating consequences, has grown to become one of the major public health nuisance of the 21st century due to the increasing number of the global population living with the disease as well as the mortality and morbidity rates accrued to the disease. One of the main approaches used in treating diabetes involves the inhibition of alpha glucosidase and alpha amylase enzymes. These enzymes are domicile in the saliva, pancreatic juice and mucosal brush border of the small

intestine are extensively involved in the breakdown of carbohydrate and polysaccharides into absorbable smaller molecules mostly glucose molecules before it is absorbed into the blood. These ultimately lead to increased glucose concentration in the blood.[68] As such, suppressing the activity of these two enzymes essentially reduces the amount of absorbable glucose concentration in the blood, which consequently reduces postprandial blood glucose level. Inhibition of these enzymes (alpha-glucosidase and alpha-amylase) is one of the effective regimens in the treatment of diabetes.[69,70] The results from the evaluation of the in vitro antidiabetic effects of SISE AgNPs is shown in Figure 6. As can be seen, SISE AgNPs displayed potent alpha-amylase and alpha-glucosidase inhibition activity at concentrations ranging from of 0.2–1.4 μg/mL. The percentage inhibition of alpha-amylase ranged between 5.3–100% at 0.2–1.4 μg/mL (Figure 6A); while the percentage inhibition for alpha-glucosidase enzyme was between 9–100% (Figure 6B).

Hg^{2+} Sensing Using SISE AgNPs

The detection and monitoring of toxic and hazardous metal ion especially Hg^{2+} is important in view of the possible effects of Hg^{2+} on human, health and the environment. As shown in Figure 7, the addition of different concentrations of Hg^{2+} to the colloidal solution of SISE AgNPs, the absorption spectra blue shifted, with a reduction in intensity, in a concentration dependent fashion (Figure 7A). Moreover, the sparkling yellow color of SISE AgNPs, progressively faded and finally
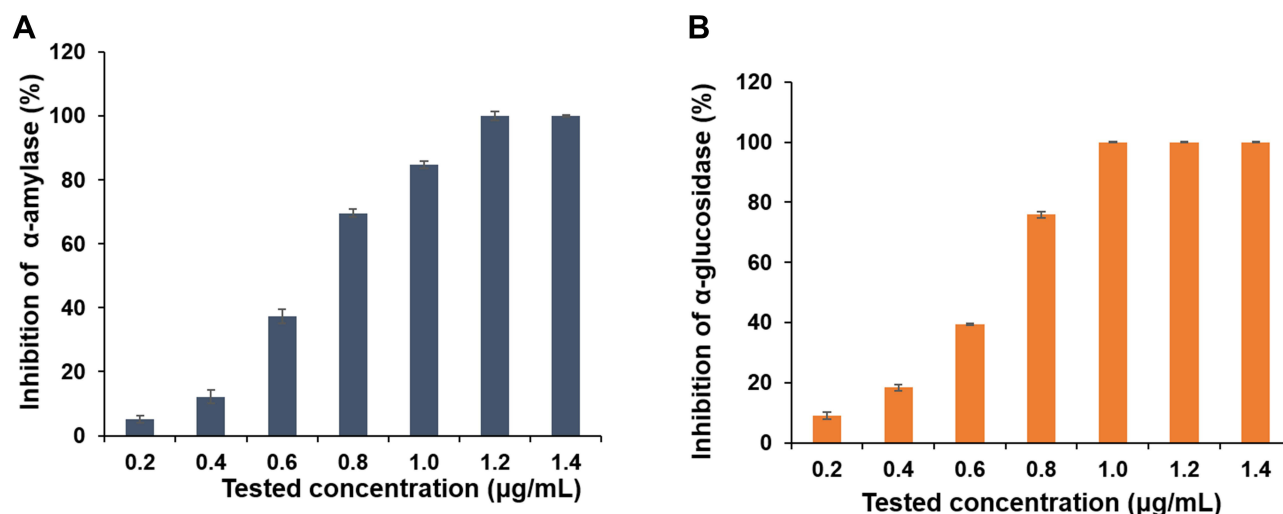
A

B

Figure 6 In vitro antidiabetic potentials of SISE AgNPs on (**A**) α-amylase and (**B**) α-glucosidase.

A

Hg^{2+}
0.0 → 60.0 μM

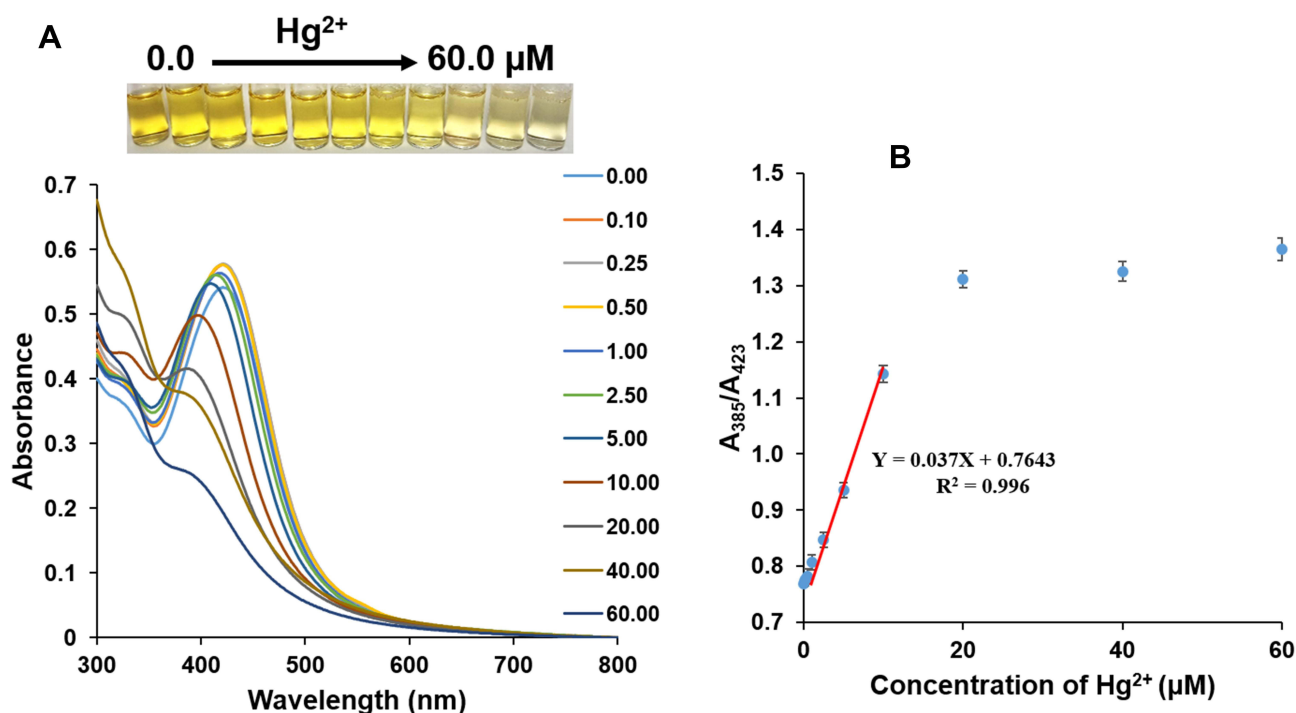**B**

$$Y = 0.037X + 0.7643$$
$$R^2 = 0.996$$

Figure 7 (**A**) UV-V is absorption spectra of SISE AgNPs, in the presence of Hg^{2+} ranging from 0.0–60.0 μM, inset shows the photo images of the various concentrations and (**B**) Plot of absorbance ratio A_{385}/A_{423} against Hg^{2+} concentrations.

turned colorless at the very high concentrations of Hg^{2+}, (Figure 7A inset). This showed that SISE AgNPs can conveniently serve as a detection probe for efficacious monitoring of toxic heavy metal in aqueous environment. As mentioned above, on addition of different concentrations of Hg^{2+}, SISE AgNPs blue shifted from absorbance maximum at 423 nm to as much as 385 nm. The sensitivity (a measure of change in analyte response

to concentration) of Hg^{2+} was obtained from the plot of A_{385}/A_{423} versus Hg^{2+} concentration, as shown in Figure 7B. The ratio increased with the concentration of Hg^{2+}, then plateaued at 20.0 μM. There existed a linear range between A_{385}/A_{423} versus Hg^{2+} concentration from 0.10–10.0 μM. The calibration plot can be fitted into the equation, $A_{385}/A_{423} = 0.037[Hg^{2+}] + 0.7643$, ($R^2=0.996$). To our knowledge using this ratio furnished better linear

range than using the more popular absorbance decrease at a single point.

The limit of detection (LOD) and limit of quantification (LOQ), which are central to analytical method design, was calculated using the equations, $3.3S_{(y/x)}$/slope and $10S_{(y/x)}$/slope, respectively. $S_{(y/x)}$ was evaluated from the standard deviation of the regression, while slope is from the calibration plot (ICH, 1996).[71] The LOD and LOQ of our SISE AgNPs towards Hg^{2+} detection was calculated to be 26.5 and 93.7 nM, respectively.

Mechanism of Hg^{2+} Detection Based on SISE AgNPs

The mechanistic basis of Hg^{2+} reaction with SISE AgNPs, causing changes in the absorption spectra and naked eye

visible color perturbation is explained, as shown in Figure 8A. The fabricated SISE AgNPs is stable in aqueous environment owing to the numerous SISE bioactive materials serving as stabilizers. The addition of Hg^{2+} will facilitate the rapid attachment/adsorption of Hg^{2+} to the negatively charged SISE AgNPs surfaces, to induce redox reaction between AgNPs (Ag^0) and Hg^{2+}. In the process, the multitudinous SISE stabilizers on the nanoparticles are damaged. The standard electrode potentials of the metals are given as, [$E^o_{Hg2+/Hg0}$ = 0.85 V] and [$E^o_{Ag+/Ag0}$ = 0.80 V].[72] Accordingly, Hg^{2+} will oxidize Ag^0 to furnish Hg^0 and Ag^+, while it is also reduced, in the process. The progressive loss of SISE AgNPs color intensity on Hg^{2+} injection is a testament to the degradation/disintegration of the formed nanoparticles, as shown in the proposed
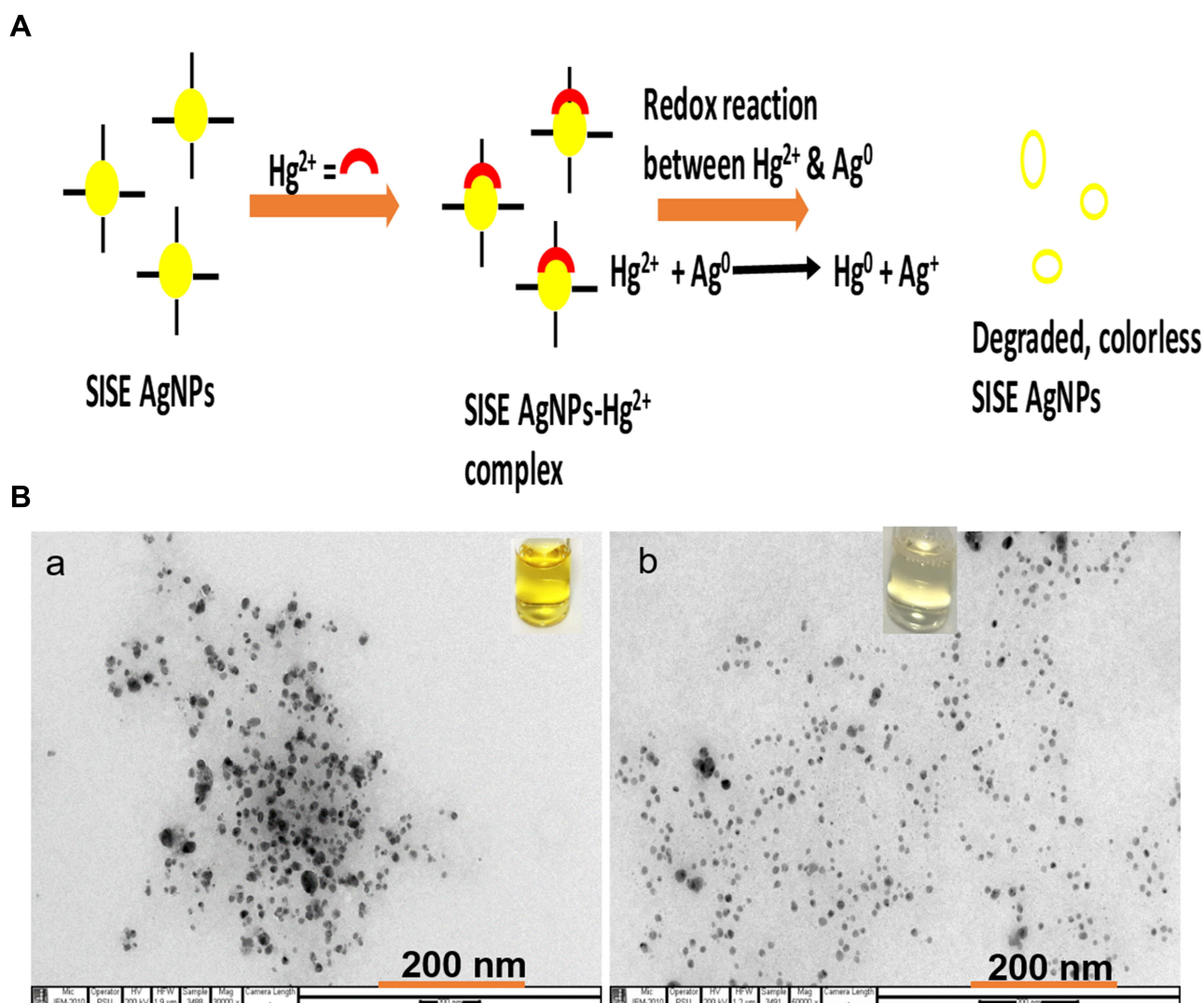

Figure 8 (**A**) Mechanistic basis of Hg^{2+} interaction with SISE AgNPs and (**B**) TEM images of (a) SISE AgNPs in the absence and (b) in the presence of 20.0 μM Hg^{2+} inset shows the photo images.

mechanism. This was further probed, by investigating the TEM images of SISE AgNPs in the absence and presence of Hg^{2+}. Figure 8B shows the TEM images of SISE AgNPs without Hg^{2+} (Figure 8B(a)). The particles are round and well ordered, while color of the solution is depicted in Figure 8B(a) inset. However, on adding 20.0 μM, Hg^{2+} to SISE AgNPs, the particles are clearly observed to be degraded (Figure 8B(b)), which laid further credence to the mechanism, that Hg^{2+} initiated redox degradation of SISE AgNPs, with concomitant loss of the nanoparticles. In fact, quite a few related works have been reported based on this mechanism for Hg^{2+} detection in aqueous environment.[73–76]

Precision of SISE AgNPs Probe Towards Hg^{2+} Detection

The precision was expressed in terms of relative standard deviation (%RSD) by estimating the response of Hg^{2+} at 0.5 and 5.0 μM, for the same day (n = 9) and for three consecutive days, in order to express the intra- and inter-day precisions. The RSD was 3.7% for intra-day precision and 4.4% for the inter-day precision. This showed that SISE AgNPs could serve as detection probe for Hg^{2+} determination with reliable reproducibility.

Selectivity of SISE AgNPs Towards Hg^{2+}

The selectivity of the probe to Hg^{2+} in comparison with other potential interfering metal ions was estimated by charging 20.0 μM, Hg^{2+} and comparing with other interfering metal ions at 50.0 μM, as shown in Figure S7. Accordingly, only the addition of Hg^{2+} could manifest in appreciable decrease in absorption spectra, with a blue shift in absorbance maximum. Further, the yellow color of SISE AgNPs was retained after the addition of other metal ions, while it turned almost colorless in the presence of Hg^{2+} (Figure S9A inset). Moreover, there was a significant increment in A_{385}/A_{423} ratio in comparison with the blank sample, even when other metal ions were about 2.5-fold higher than Hg^{2+} concentration (Figure S9B). This is owing to the fact that only Hg^{2+} could initiate the oxidative etching effect on SISE AgNPs. This shows the method can be selective for practical determination of Hg^{2+} in complex samples.

Comparison of SISE AgNPs with Reported Works for Hg^{2+} Detection

The comparison of SISE AgNPs probe with other reported detection strategy for Hg^{2+} is shown in Table S3. As can

be observed, the analytical figures of merit obtained from the use of SISE AgNPs for the detection of Hg^{2+} is comparable or better than some of the reported methods. It is worth emphasizing, however, that while highly toxic reductants were used for the synthesis of some of the reported probes, the use of SISE in this work is exhilarating in terms of its use as an eco-friendly bio resource, to further deepen the "green research" concept.

Real Sample Application of SISE AgNPs for Hg2+ Detection

The practicality of SISE AgNPs for Hg^{2+} detection in real sample was demonstrated by performing Hg^{2+} determination using the Prince of Songkla University, Hatyai, Thailand, wastewater reservoir. The sample was collected and processed by boiling, cooling, centrifuging and passing through a membrane filter of 0.22-micron size. The standard addition technique was used for Hg^{2+} estimation on the sample, by spiking different concentrations of Hg^{2+} into the processed water sample. Then the detection assay was carried out as explained above. The final concentration of Hg^{2+} (0.25, 1.0 and 5.0 μM), were estimated using the calibrated plot. Accordingly, the percent recovery (Found/Added × 100) estimated is shown in Table 2, which ranged between 95.6–102.7%. The recovery estimated revealed that SISE AgNPs can be reliably applied for Hg^{2+} determination in real environmental sample.

Conclusion

In this work, *Securidaca inappendiculata* stem extract (SISE), has been investigated as an eco-friendly bio resource for the reduction and stabilization of silver nanoparticles (AgNPs), at room temperature. SISE was found to be rich in bioactive components which facilitated the synthesis of AgNPs almost instantaneously. The synthesized SISE AgNPs was investigated for wide spectrum biological applications, ranging from antioxidant,

Table 2 Real Sample Application of SISE AgNPs Towards Hg^{2+} Detection in Water, (n = 3)

Concentration Hg^{2+} (μM)		Recovery (%)	RSD (%)
Added	Found		(n = 3)
0	0.0	–	–
0.25	0.239 ± 0.025	95.6	1.8
1.00	0.98 ± 0.065	98.0	3.4
5.00	5.13 ± 0.25	102.6	2.9

antibacterial, hemolytic, cyto-compatibility and antidia-betic potentiality. SISE AgNPs was found to possess good in-vitro performances for the aforementioned assays, which may be a positive reality, towards more detailed applications of SISE in the biomedical field. Since the human biological system may be the final sink for Hg^{2+} exposure from the environment, the need for consistent monitoring of Hg^{2+} in environmental samples cannot be over-emphasized. Consequently, we further exploited the capacity of our synthesized SISE AgNPs as an optical probe towards the detection of Hg^{2+} in aqueous environ-ment, with exciting analytical performances. SISE AgNPs demonstrated linearity within 0.10–10.0 μM, with a limit of detection of 26.5 nm, when investigated for Hg^{2+} detec-tion. On comparison with other potential interfering metal ions, SISE AgNPs was found to be highly selective towards Hg^{2+}, which further accentuated the prospect of the probe in practical monitoring of toxic heavy metal of interest. Finally, we demonstrated the use of SISE AgNPs for Hg^{2+} determination in real sample, with good accuracy and precision. In all, SISE AgNPs presented positive potentiality to serve as a multifaceted nanomaterial, with intrinsic capacity to function for diverse applications.

Highlights

- *Securidaca inappendiculata* stem extract (SISE), was used as the reductant and stabilizing agent for silver nanoparticles synthesis at room temperature.
- SISE AgNPs were of average size 10–15 nm, with zeta value of −19.5 ± 1.8 mV.
- SISE AgNPs was tested for different biological assays (antioxidants, antibacterial, biocompatibility and antidiabetic).
- SISE AgNPs was applied as optical probe for Hg^{2+} detection, with limit of detection of 26.5 nM.
- SISE AgNPs could detect Hg^{2+} in wastewater sample with good accuracy.

Abbreviations

SISE, *Securidaca inappendiculata* stem extract; SISE AgNPs, synthesized silver nanoparticles from SISE; Hg^{2+}, mercury (II) ion; RT, room temperature.

Acknowledgments

Disclosure

The authors report no conflicts of interest for this work.

References

1. International Organization for Standardization. *Nanotechnologies-Vocabulary- Part 1: Core Terms. ISO/TS 80004-1:2015(En)*. International Organization for Standardization; 2015.
2. Zhang XF, Liu ZG, Shen W, et al. Silver nanoparticles: synthesis, characterization, properties, applications, and therapeutic approaches. *Inter J Mol Sci*. 2016;17(9):1534. doi:10.3390/ijms17091534
3. Agostino RG, Donato S, Caruso T, et al. Microtomographic studies as a tool in the identification of a new ceramic class: the metal-imitating pottery as grave goods among Brettians and Lucanians. *Microchem J*. 2016;126:138–148. doi:10.1016/j.microc.2015.12.007
4. Mavani K, Shah M. Synthesis of silver nanoparticles by using sodium borohydride as a reducing agent. *Inter J Eng Res Technol*. 2013;2(3):1–5.
5. Gurusamy V, Krishnamoorthy R, Gopal B, et al. Systematic investi-gation on hydrazine hydrate assisted reduction of silver nanoparticles and its antibacterial properties. *Inorg Nano Met Chem*. 2017;47(5):761–767. doi:10.1080/15533174.2015.1137074
6. Pastoriza-Santos I, Liz-Marzán KM. Reduction of silver nanoparti-cles in DMF. Formation of monolayers and stable colloids. *Pure Appl Chem*. 2000;72(1–2):83–90. doi:10.1351/pac200072010083
7. Das G, Patra JK, Shin HS. Biosynthesis, and potential effect of fern mediated biocompatible silver nanoparticles by cytotoxicity, antidia-betic, antioxidant and antibacterial, studies. *Mater Sci Eng C*. 2020;114:111011. doi:10.1016/j.msec.2020.111011
8. Moldovan B, David L, Vulcu A, et al. In vitro and in vivo anti-inflammatory properties of green synthesized silver nanoparticles using *Viburnum opulus* L. fruits extract. *Mater Sci Eng C*. 2017;79:720–727. doi:10.1016/j.msec.2017.05.122
9. Eze FN, Tola AJ, Nwabor OF, et al. *Centella asiatica* phenolic extract-mediated bio-fabrication of silver nanoparticles: characteriza-tion, reduction of industrially relevant dyes in water and antimicro-bial activities against foodborne pathogens. *RSC Adv*. 2019;9(65):37957–37970. doi:10.1039/C9RA08618H
10. Morales-Lozoya V, Espinoza-Gómez H, Flores-López LZ, et al. Study of the effect of the different parts of Morinda citrifolia L. (noni) on the green synthesis of silver nanoparticles and their antibacterial activity. *Appl Surf Sci*. 2021;537:147855. doi:10.1016/j.apsusc.2020.147855
11. Elemike EE, Onwudiwe DC, Ekennia AC, et al. Phytosynthesis of silver nanoparticles using aqueous leaf extracts of Lippia citriodora: antimicrobial, larvicidal and photocatalytic evaluations. *Mater Sci Eng C*. 2017;75:980–989. doi:10.1016/j.msec.2017.02.161
12. Perni S, Hakala V, Prokopovich P. Biogenic synthesis of antimicro-bial silver nanoparticles capped with l-cysteine. *Colloids Surf A: Physicochem Eng Asp*. 2014;460:219–224. doi:10.1016/j.colsurfa.2013.09.034
13. Eze FN, Nwabor OF. Valorization of Pichia spent medium via one-pot synthesis of biocompatible silver nanoparticles with potent antioxidant, antimicrobial, tyrosinase inhibitory and reusable catalytic activities. *Mater Sci Eng C*. 2020;115:111104. doi:10.1016/j.msec.2020.111104
14. Maddinedi SB, Mandal BK, Anna KK. Tyrosine assisted size-controlled synthesis of silver nanoparticles and their catalytic, in-vitro cytotoxicity evaluation. *Environ Toxicol Pharmacol*. 2017;51:23–29. doi:10.1016/j.etap.2017.02.020
15. Jayeoye TJ, Rujiralai T. Green, in situ fabrication of silver/poly (3-aminophenyl boronic acid)/sodium alginate nanogel and hydrogen peroxide sensing capacity. *Carbohydr Polym*. 2020;246:116657. doi:10.1016/j.carbpol.2020.116657

16. Jayeoye TJ, Nwabor OF, Rujiralai T. Synthesis of highly stable and dispersed silver nanoparticles/poly (vinyl alcohol-co-ethylene glycol)/poly (3-aminophenyl boronic acid) nanocomposite: characterization and antibacterial, hemolytic and cytotoxicity studies. *J Ind Eng Chem*. 2020;89:288–300. doi:10.1016/j.jiec.2020.05.025

17. Benassai E, Del Bubba M, Ancillotti C, et al. Green and cost-effective synthesis of copper nanoparticles by extracts of non-edible and waste plant materials from Vaccinium species: characterization and antimicrobial activity. *Mater Sci Eng C*. 2020;119:111453. doi:10.1016/j.msec.2020.111453

18. Chawla P, Kumar N, Bains A, et al. Gum Arabic capped copper nanoparticles: synthesis, characterization, and applications. *Inter J Biol Macromol*. 2020;146:232–242. doi:10.1016/j.ijbiomac.2019.12.260

19. Yousaf H, Mehmood A, Ahmad KS, et al. Green synthesis of silver nanoparticles and their applications as an alternative antibacterial and antioxidant agent. *Mater Sci Eng C*. 2020;112:110901. doi:10.1016/j.msec.2020.110901

20. He Y, Li H, Fei X, et al. Carboxymethyl cellulose/cellulose nanocrystals immobilized silver nanoparticles as an effective coating to improve barrier and antibacterial properties of paper for food packaging applications. *Carbohydr Polym*. 2020;252:117156. doi:10.1016/j.carbpol.2020.117156

21. Syukri DM, Nwabor OF, Singh S, et al. Antibacterial-coated silk surgical sutures by ex situ deposition of silver nanoparticles synthesized with Eucalyptus camaldulensis eradicates infections. *J Microbiol Methods*. 2020;174:105955. doi:10.1016/j.mimet.2020.105955

22. Ghosh S, Mondal A. Aggregation chemistry of green silver nanoparticles for sensing of Hg2+ and Cd2+ ions. *Colloids Surf A: Physicochem Eng Asp*. 2020;605:125335. doi:10.1016/j.colsurfa.2020.125335

23. Al-Thabaiti SA, Khan Z. Biogenic synthesis of silver nanoparticles, sensing and photo catalytic activities for bromothymol blue. *J Photochem Photobiol*. 2020;3:100010. doi:10.1016/j.jpap.2020.100010

24. Gul AR, Shaheen F, Rafique R, et al. Grass-mediated biogenic synthesis of silver nanoparticles and their drug delivery evaluation: a biocompatible anti-cancer therapy. *Chem Eng J*. 2020;407:127202. doi:10.1016/j.cej.2020.127202

25. Ameen F, Alsamhary K, Alabdullatif JA, et al. A review on metal-based nanoparticles and their toxicity to beneficial soil bacteria and fungi. *Ecotoxicol Environ Saf*. 2021;213:112027. doi:10.1016/j.ecoenv.2021.112027

26. Kumar S, Jha I, Mogha NK, et al. Biocompatibility of surface-modified gold nanoparticles towards red blood cells and haemoglobin. *Appl Surf Sci*. 2020;512:145573. doi:10.1016/j.apsusc.2020.145573

27. Zha H, Wang Z, Yang X, et al. New acylated triterpene saponins from the roots of *Securidaca inappendiculata* Hassk. *Phytochem Lett*. 2015;13:108–113. doi:10.1016/j.phytol.2015.05.022

28. Jiang H, Ji CL, Yang K, et al. Fatty oil from Securidaca inappendiculata exerted therapeutic effects on adjuvant-induced arthritis in mice via suppression on fibroblast-like synoviocyte. *Kaohsiung J Med Sci*. 2018;34(11):616–625. doi:10.1016/j.kjms.2018.06.007

29. Zuo J, Ji CL, Xia Y, et al. Xanthones as α -glucosidase inhibitors from the antihyperglycemic extract of Securidaca inappendiculata. *Pharm Biol*. 2014;52(7):898–903. doi:10.3109/13880209.2013.872673

30. Zuo J, Ji CL, Olatunji OJ, et al. Bioactive fractions from *Securidaca inappendiculata* alleviated collagen-induced arthritis in rats by regulating metabolism-related signaling. *Kaohsiung J Med Sci*. 2020;36 (7):523–534. doi:10.1002/kjm2.12205

31. Ji J, Wang Q, Wang M, et al. Chemical constituents from the stems of *Securidaca inappendiculata* Hassk. *Fitoterapia*. 2019;137:104271. doi:10.1016/j.fitote.2019.104271

32. Li Z, Chen B, Li Y, et al. Reduction of mercury emissions from anthropogenic sources including coal combustion. *J Environ Sci*. 2021;100:363–368. doi:10.1016/j.jes.2020.11.002

33. UNEP. *Toolkit for Identification and Quantification of Mercury Releases. IMOC—Inter Organizational Programme for the Sound Management of Chemicals. A Cooperative Agreement Among UNEP, ILO, FAO, WHO, UNIDO*. Geneva, Switzerland: UNITAR and OECD; 2005:282.

34. Wang L, Hou D, Cao Y, et al. Remediation of mercury contaminated soil, water, and air: a review of emerging materials and innovative technologies. *Environ Int*. 2020;134:105281. doi:10.1016/j.envint.2019.105281

35. Tao H, Hu T, Yan J, et al. A comparative study of different reagentless plasmon sensors based on Ag–Au alloy nanoparticles for detection of Hg. *Sens Actuators B: Chem*. 2015;208:43–49. doi:10.1016/j.snb.2014.11.003

36. Liu J, Feng X, Zhu W, et al. Spatial distribution and speciation of mercury and methyl mercury in the surface water of East River (Dongjiang) tributary of Pearl River Delta, South China. *Environ Sci Pollut Res*. 2012;19(1):105–112. doi:10.1007/s11356-011-0542-0

37. Eze FN, Leelawatwattana L, Prapunpoj P. Structural stabilization of human transthyretin by Centella asiatica (L.) urban extract: implications for TTR amyloidosis. *Biomolecules*. 2019;9(4):128. doi:10.3390/biom9040128

38. Olatunde OO, Benjakul S, Vongkamjan K. Coconut husk extract: antibacterial properties and its application for shelf-life extension of Asian sea bass slices. *Inter J Food Sci Technol*. 2019;54(3):810–822. doi:10.1111/ijfs.14000

39. Amin K, Dannenfelser RM. In vitro hemolysis: guidance for the pharmaceutical scientist. *J Pharm Sci*. 2006;95:1173–1176. doi:10.1002/jps.20627

40. Jana SK, Mandal AK, Kumar A, et al. Sensing of tryptophan by a non-toxic cobalt(ii) complex. *RSC Adv*. 2016;6(98):95888–95896. doi:10.1039/C6RA16086G

41. Chakrabarti R, Singh B, Prakrith VN, et al. Screening of nine herbal plants for in vitro α-amylase inhibition. *Asian J Pharm Clin Res*. 2014;7:84–89.

42. Sudha P, Zinjarde SS, Bhargava SY, et al. Potent α-amylase inhibitory activity of Indian Ayurvedic medicinal plants. *BMC Compl Alt Med*. 2011;11:1–10. doi:10.1186/1472-6882-11-5

43. Kumar S, Kumar V, Prakash O. Enzymes inhibition and antidiabetic effect of isolated constituents from Dillenia indica. *Biomed Res Inter*. 2013;2013:382063. doi:10.1155/2013/382063

44. Bhutto AA, Kalay S, Sherazi STH, et al. Quantitative structure–activity relationship between antioxidant capacity of phenolic compounds and the plasmonic properties of silver nanoparticles. *Talanta*. 2018;189:174–181. doi:10.1016/j.talanta.2018.06.080

45. Olatunji OJ, Zuo J, Olatunde OO. *Securidaca inappendiculata* stem extract confers robust antioxidant and antidiabetic effects against high fructose/streptozotocin induced type 2 diabetes in rats. Exploration of bioactive compounds using UHPLC-ESI-QTOF-MS. *Arch Physiol Biochem*. 2021;1–13. doi:10.1080/13813455.2021.1921811

46. SKim SB, Chang BY, Han SB, et al. A new phenolic glycoside from *Cnidium monnieri* fruits. *Nat Prod Res*. 2013;27:1945–1948. doi:10.1080/14786419.2013.796467

47. Cheriet T, Ben-Bachir B, Thamri O, et al. Isolation and biological properties of the natural flavonoids pectolinarin and pectolinarigenin-a review. *Antibiotics*. 2020;9(7):417. doi:10.3390/antibiotics9070417

48. Navarro JR, Werts MH. Resonant light scattering spectroscopy of gold, silver and gold–silver alloy nanoparticles and optical detection in microfluidic channels. *Analyst*. 2013;138(2):583–592. doi:10.1039/c2an36135c

49. Thanh NT, Maclean N, Mahiddine NS. Mechanisms of nucleation and growth of nanoparticles in solution. *Chem Rev*. 2014;114 (15):7610–7630. doi:10.1021/cr400544s

50. Jayeoye TJ, Sirimahachai U, Rujiralai T. Sensitive colorimetric detection of ascorbic acid based on seed mediated growth of sodium alginate reduced/stabilized gold nanoparticles. *Carbohydr Polym*. 2020;255:117376. doi:10.1016/j.carbpol.2020.117376

51. Okaiyeto K, Ojemaye MO, Hoppe H, et al. Phytofabrication of silver/silver chloride nanoparticles using aqueous leaf extract of Oedera genistifolia: characterization and antibacterial potential. *Molecules*. 2019;24(23):4382. doi:10.3390/molecules24234382

52. Jayeoye TJ, Eze FN, Olatunde OO, et al. Synthesis of silver and silver@ zero valent iron nanoparticles using Chromolaena odorata phenolic extract for antibacterial activity and hydrogen peroxide detection. *J Environ Chem Eng*. 2021;9(3):105224. doi:10.1016/j.jece.2021.105224

53. Lobo V, Patil A, Phatak A, et al. Free radicals, antioxidants and functional foods: impact on human health. *Pharmacogn Rev*. 2010;4(8):118. doi:10.4103/0973-7847.70902

54. Melinda KP, Rathinam X, Marimuthu K, et al. A comparative study on the antioxidant activity of methanolic leaf extracts of *Ficus religiosa* L, *Chromolaena odorata* (L.) King & Robinson, *Cynodon dactylon* (L.) Pers. and *Tridax procumbens* L. *Asian Pac J Trop Med*. 2010;3(5):348–350. doi:10.1016/S1995-7645(10)60084-3

55. El-Batal AI, Mosalam FM, Ghorab M, et al. Antimicrobial, antioxidant and anticancer activities of zinc nanoparticles prepared by natural polysaccharides and gamma radiation. *Int J Biol Macromol*. 2018;107:2298–2311. doi:10.1016/j.ijbiomac.2017.10.121

56. De Souza RF, De Giovani WF. Antioxidant properties of complexes of flavonoids with metal ions. *Redox Rep*. 2004;9(2):97–104. doi:10.1179/135100004225003897

57. Abbaszadegan A, Ghahramani Y, Gholami A, et al. The effect of charge at the surface of silver nanoparticles on antimicrobial activity against gram-positive and gram-negative bacteria: a preliminary study. *J Nanomater*. 2015;16(1):53. doi:10.1155/2015/720654

58. Shams S, Khan AU, Yuan Q, et al. Facile and eco-benign synthesis of Au@ Fe2O3 nanocomposite: efficient photocatalytic, antibacterial and antioxidant agent. *J Photochem Photobiol B: Biol*. 2019;199:111632. doi:10.1016/j.jphotobiol.2019.111632

59. Geethadevi R, Maheshwari V. Imparting antimicrobial finish on selected regenerated cellulosic fabrics with herbal oil combinations. *J Text Sci Eng*. 2013;4(144):1. doi:10.4172/2165-8064.1000144

60. Olatunde OO, Benjakul S, Vongkamjan K. Antioxidant and antibacterial properties of guava leaf extracts as affected by solvents used for prior dechlorophyllization. *J Food Biochem*. 2018;42(5):12600. doi:10.1111/jfbc.12600

61. Qais FA, Shafiq A, Khan HM, et al. Antibacterial effect of silver nanoparticles synthesized using *Murraya koenigii* (L.) against multidrug-resistant pathogens. *Bioinorg Chem Appl*. 2019;2019:1–11. doi:10.1155/2019/4649506

62. Jayeoye TJ, Olatunde OO, Benjakul S, et al. Synthesis and characterization of novel poly (3-aminophenyl boronic acid-co-vinyl alcohol) nanocomposite polymer stabilized silver nanoparticles with antibacterial and antioxidant applications. *Colloids Surf B: Biointerfaces*. 2020;193:111112. doi:10.1016/j.colsurfb.2020.111112

63. Acharya D, Singha JM, Pandey P, et al. Shape dependent physical mutilation and lethal effects of silver nanoparticles on bacteria. *Sci Rep*. 2018;8(1):201. doi:10.1038/s41598-017-18590-6

64. Preté PSC, Domingues CC, Meirelles NC, et al. Multiple stages of detergent-erythrocyte membrane interaction—a spin label study. *Biochim Biophys Acta Biomembr*. 2011;1808:164–170. doi:10.1016/j.bbamem.2010.10.016

65. Rawlinson LAB, O'Brien PJ, Brayden DJ. High content analysis of cytotoxic effects of pDMAEMA on human intestinal epithelial and monocyte cultures. *J Control Release*. 2010;146:84–92. doi:10.1016/j.jconrel.2010.05.002

66. Attarilar S, Yang J, Ebrahimi M, et al. The toxicity phenomenon and the related occurrence in metal and metal oxide nanoparticles: a brief review from the biomedical perspective. *Front Bioeng Biotechnol*. 2020;8. doi:10.3389/fbioe.2020.00822

67. Nwabor OF, Singh S, Ontong JC, et al. Valorization of wastepaper through antimicrobial functionalization with biogenic silver nanoparticles, a sustainable packaging composite. *Waste Biomass Valori*. 2021;12(6):3287–3301. doi:10.1007/s12649-020-01237-5

68. Makinde EA, Ovatlarnporn C, Adekoya EA, et al. Antidiabetic, antioxidant and antimicrobial activity of the aerial part of *Tiliacora triandra*. *S Afr J Bot*. 2019;125:337–343. doi:10.1016/j.sajb.2019.08.012

69. Kasipandi M, Manikandan A, Sreeja PS, et al. Effects of in vitro simulated gastrointestinal digestion on the antioxidant, α-glucosidase and α-amylase inhibitory activities of water-soluble polysaccharides from Opilia amentacea roxb fruit. *LWT Food Sci Technol*. 2019;111:774–781. doi:10.1016/j.lwt.2019.05.079

70. Rizvi TS, Hussain I, Ali L, et al. New gorgonane sesquiterpenoid from Teucrium mascatense Boiss, as α-glucosidase inhibitor. *S Afr J Bot*. 2019;124:218–222. doi:10.1016/j.sajb.2019.05.008

71. ICH. International Conference on Harmonization of Technical Requirements for Registration of Pharmaceuticals for Human Use, Q2B Validation of Analytical Procedures: Methodology, ICH-Q2B; 1996:1–10.

72. Bard AJ, Parson R, Jordan J. *Standard Potentials in Aqueous Solution, International Union of Pure and Applied Chemistry*. New York: Marcel Dekker Inc; 1985.

73. Choudhary MK, Garg S, Kaur A, et al. Green biomimetic silver nanoparticles as invigorated colorimetric probe for Hg^{2+} ions: a cleaner approach towards recognition of heavy metal ions in aqueous media. *Mater Chem Phys*. 2020;240:122164. doi:10.1016/j.matchemphys.2019.122164

74. Bandi R, Alle M, Park C, et al. Rapid synchronous synthesis of Ag nanoparticles and Ag nanoparticles/holocellulose nanofibrils: Hg (II) detection and dye discoloration. *Carbohydr Polym*. 2020;240:116356. doi:10.1016/j.carbpol.2020.116356

75. Sakly N, Marzouk W, Ouada HB, et al. Enhancing performances of colorimetric response of carboxymethylcellulose-stabilized silver nanoparticles: a fully eco-friendly assay for Hg2+ detection. *Sens Actuators B: Chem*. 2017;253:918–927. doi:10.1016/j.snb.2017.07.035

76. Borase HP, Patil CD, Salunkhe RB, et al. Mercury sensing and toxicity studies of novel latex fabricated silver nanoparticles. *Bioprocess Biosyst Eng*. 2014;37(11):2223–2233. doi:10.1007/s00449-014-1200-y